Vol. 34 (2003) *ACTA PHYSICA POLONICA B* No 8

STUDY OF HIGH MASS HIGGS USING $pp \to qqH$

H.D. Yildiz[†]

Physics Department, Dumlupinar University, Kutahya, Turkey

and M.T. Zeyrek

Physics Department, Middle East Technical University
Ankara 06531, Turkey
e-mail: hyildiz@newton.physics.metu.edu.tr

(Received January 30, 2003; revised version received June 6, 2003)

The observability of the Higgs signal in the mass range of 200–800 GeV is investigated in the weak boson fusion channel at the CMS experiment at LHC. The weak boson fusion channel is characterized by two final state jets at large pseudorapidity. The forward calorimeter plays a key role in detecting these jets. The significant signals are obtained for $H \to WW \to l\nu jj$, $H \to ZZ \to lljj$ and $H \to ZZ \to ll\nu\nu$. Importance of the forward jet tagging and the central jet veto is emphasized to extract the signal from the large QCD $W/Z+$ jets and the top backgrounds. This analysis shows that the Higgs particle with mass 300 GeV to 800 GeV can be observed in WW and ZZ decay channels with an integrated luminosity of about 10 to 20 fb^{-1} in the low luminosity running conditions in CMS.

PACS numbers: 14.80.Bn

1. Introduction

One of the main objectives of the LHC experiments is to discover the Higgs particle. LEP II sets a lower bound at around 114.1 GeV for the Standard Model Higgs [1]. The indirect searches, performing fits to all existing electroweak data indicate a light Standard Model Higgs [2]. However higher mass values for the Higgs should also be included for the LHC sensitivity measurements.

The CMS collaboration has established the expected discovery ranges for the most important production and decay channels of the Standard and

[†] This work has been performed in the context of this author's Ph.D. thesis at METU-Ankara.

Supersymmetric Model Higgs Bosons. For the Standard Model Higgs $H \to ZZ \to 4l^{\pm}$ provides an excellent signature over a large mass range from $m_H \sim 130$ GeV to $m_H \sim 500$ GeV. $H \to \gamma\gamma$ and $H \to b\bar{b}$ are the main discovery channels for the low mass region $m_H \leq 120$ GeV, but it may require several years of running for a discovery. In recent years, to strengthen the discovery potential of the production of the Standard Model Higgs boson in the weak boson fusion channels and their subsequent decays to $H \to \gamma\gamma$, $H \to \tau\tau$ and $H \to WW$ have been studied.

In this study we report the observability of Higgs signal in the mass range from 200 GeV to 800 GeV in the weak boson fusion channels in Eqs. (1)–(3) as a complementary channel to $H \to ZZ \to 4l^{\pm}$ at the CMS experiment. The Higgs mass of $m_H < 200$ GeV can also be investigated in the weak boson channel in the decay mode of $H \to WW^* \to l\nu l\nu$ [8, 13]. The weak boson channels then provide a complete study of the possible Higgs observation over a wide range of masses at the CMS experiment.

Although the gluon–gluon fusion dominates for the Higgs production for the entire mass range, weak boson fusion has still a sizeable fraction of the total cross section for all relevant Higgs masses. The characteristics of the weak boson fusion mechanism is the presence of the energetic forward jets separated at large pseudorapidity. The hadronic jet activity in the central region is then dominantly suppressed. This kinematical feature brings a good reduction of the QCD and the top backgrounds.

The forward jets are most populated at $|\eta| \approx 3$. Nearly half of these tagged jets are detected by the forward calorimeter (HF) which covers the pseudorapidity range $3 \leq |\eta| \leq 5$, the other half by the endcap electromagnetic (EE), and the endcap hadronic calorimeter (HE) of CMS [3]. The HF calorimeters increase the total coverage to $|\eta| \approx 5$ and also reduce the fake (instrumental) $E_{\mathrm{t}}^{\mathrm{miss}}$.

Here we investigated principal decay modes of the Standard Model Higgs Boson through the processes $H \to WW$ and $H \to ZZ$. The reactions are:

$$
\begin{aligned}
pp &\to jjH, \quad H \to W_1 W_2, \quad W_1 \to l\nu, \quad W_2 \to jj, &(1)\\
pp &\to jjH, \quad H \to Z_1 Z_2, \quad Z_1 \to ll, \quad Z_2 \to jj, &(2)\\
pp &\to jjH, \quad H \to Z_1 Z_2, \quad Z_1 \to ll, \quad Z_2 \to \nu\nu, &(3)
\end{aligned}
$$

where leptons (l) are either electrons or muons, j stands for the jets.

$$H \to WW \to l\nu jj, \quad H \to ZZ \to lljj, \quad \text{and} \quad H \to ZZ \to ll\nu\nu$$

have been studied previously in CMS [4] and in ATLAS [5].

The previous studies for these channels in CMS considered the mass range of $m_H \geq 800$ GeV using early versions of the detector simulation software [4]. Now, the design of the CMS experiment is finalized and the simulation software is improved. In this study the fast CMS detector simulation package, CMSJET, is used and we extend the previous studies to lower mass ranges down to ~ 200 GeV for the Standard Model Higgs observation. These channels were also investigated by ATLAS for 300 GeV–1 TeV Higgs mass region [5]. The result of their study is comparable to CMS results.

Here, we show that Higgs mass can be reconstructed using the channels (1) and (2). However for the channel (3) Higgs mass cannot be reconstructed, but the signal can be observed in the missing energy spectrum.

The largest backgrounds for the weak boson fusion channel are $t\bar{t}$ and $W/Z+$jets. We considered $t\bar{t}$ and $W+$jets as backgrounds for the reaction (1) and $Z+$jets as background for the reactions (2) and (3). $W+$jets production with $W \to l\nu$ is potentially the largest background for the $H \to WW$ signal. $t\bar{t} \to WbW\bar{b} \to l\nu jjb\bar{b}$ reaction contains a real $W \to jj$ decay, but also additional hadronic activity from b jets in the central region. $Z+$jets production where Z decays to two leptons is the potential background for the $H \to ZZ$ signal. WW, ZZ productions in both electroweak and QCD processes are also backgrounds, but due to their lower rates than QCD $W/Z+$jets and $t\bar{t}$ productions, they are not considered in this analysis. WW/ZZ continuum contribution is shown to be only a few percent of the total background for $m_H > 200$ GeV in [6] and [7].

The leptonic decays of the W and Z are recognized by high transverse momentum leptons. The hadronic decays, where the W and Z fragments to jets, have a higher branching ratio but are more difficult to separate from the background. In searching Higgs boson, decaying to WW/ZZ we therefore require, at least, one W or Z decaying leptonically providing an isolated high p_{t} lepton trigger, while the other W or Z is reconstructed from its hadronic decay.

In this analysis suppression of the background is mainly achieved by forward jet selection in the final state. This selection requires one forward and one backward high energy jet in the large pseudorapidity range $|\eta| > 2$ and with a large gap between them. Fig. 1 shows the typical pseudorapidity distribution of jets in a signal, $H \to ZZ$ decay, where central jets are from one of the Z decays and forward jets are the tagged jets originated from the interaction vertex.

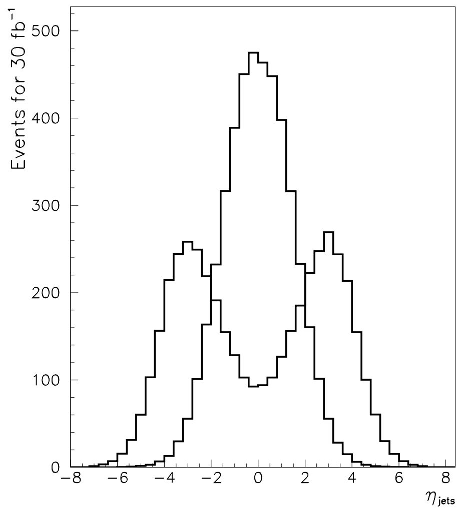

Fig. 1. The pseudorapidity, η, distributions of jets in $H \to ZZ \to lljj$. The forward jets are seen to peak at $|\eta| \approx 3$. The central jets are dominantly populated at $|\eta| < 2$.

2. Event generation and reconstruction

Signal and background events are generated by PYTHIA (6.152) [10]. Although parton shower approximation of PYTHIA provides enough information about the background processes in this study, the matrix element calculations may still be needed for some of the backgrounds [9]. The fast detector simulation package, CMSJET [11] is used for the calorimeter simulation and for the jets and missing transverse energy reconstruction. The CMSJET package simulates the CMS detector by taking into account the main cracks and detector inefficiencies. The detector resolutions are parametrized from full simulation studies. For the jet reconstruction cone we use $\Delta R = 0.5$ for m_H=600 and 800 GeV and $\Delta R = 0.7$ for m_H=200 GeV and 300 GeV over the whole calorimeter η range. We assume an overall 90% efficiency for the lepton finding efficiency. In this simulation, the low luminosity running conditions are assumed by superimposing two minimum bias events as a pile-up.

3. Analysis

In this section, we investigate three signatures in (1)–(3) for the isolation of Higgs events. In each case, we have used central cuts for leptons and jets and jet tagging cuts for forward/backward jets from the interaction.

3.1. $H \to WW \to l\nu jj$ [12]

In this case, where Higgs decays to WW with a subsequent decay of one W to $l\nu$ and the other W to jj, we have selected the events having an isolated high $p_{\rm t}^l$ lepton (electron or muon) in the central region. Fig. 2 shows the maximum $p_{\rm t}^l$ distribution for the signals and for the backgrounds. Two central jets are isolated by requiring a high transverse energy. Maximum $E_{\rm t}^{\rm jets}$ distribution for the central jets is shown in Fig. 3.

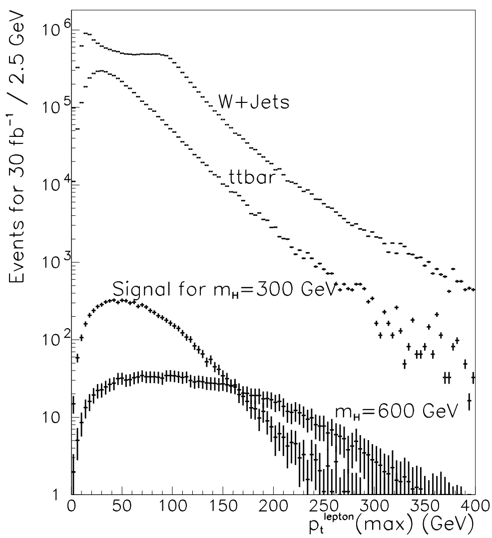

Fig. 2. Maximum $p_{\rm t}$ distribution of charged leptons for the signal $H \to WW \to l\nu jj$ and backgrounds ($t\bar{t}$ and $W + \text{jets}$) with $m_H = 300$ and $m_H = 600$ GeV.

The forward jets are identified by requiring two energetic jets (Fig. 4) with a minimum transverse energy ($E_{\rm t} > 30$ GeV) in the forward/backward region with a large pseudorapidity difference between them. The basic cuts for this channel are as follows:

$$p_{\rm t}^l > 30 \text{ GeV}, \quad |\eta_l| < 2, \tag{4}$$

$$E_{\rm t}^{\rm jets} > 40 \text{ GeV}, \quad |\eta_j| \leq 2, \quad E^{\rm tag-jet} > 300 \text{ GeV}, \quad |\eta_{\rm tag-jet}| > 2. \tag{5}$$

In the selection of forward/backward jets we also require jet–jet system to have a high invariant mass, ($M_{jj} > 1000$ GeV) and a wide separation in the η space ($\Delta\eta_{jj} > 5$) between the two jets for the better selection efficiency of the signal against the background.

We then reconstruct the mass of W's from their decay products. Two central jets are used in the reconstruction of one of the W mass. Fig. 6 (left figure) shows the reconstructed mass of W's from the central jets. The

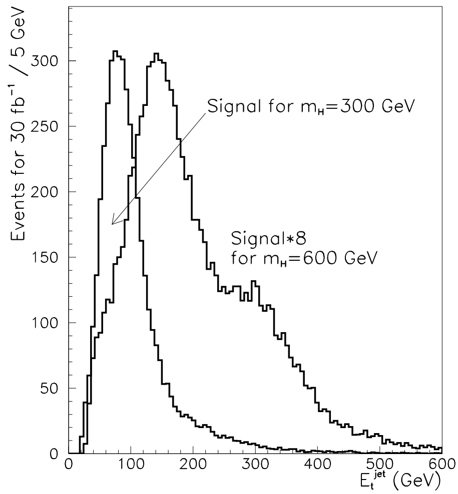

Fig. 3. Maximum transverse energy, E_{t} distribution of the central jets for the $H \to WW \to l\nu jj$ signal with $m_H = 300$ and $m_H = 600$ GeV.

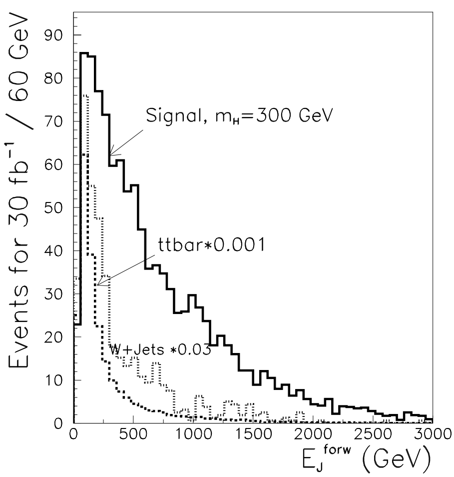

Fig. 4. Energy distributions for the forward jets in $H \to WW \to l\nu jj$ for $m_H =$ 300 GeV and for the backgrounds ($t\bar{t}$ and $W +$ jets).

other W mass is reconstructed from the charged lepton and a neutrino. The longitudinal component of the neutrino momentum in the reaction $W \to l\nu$ is estimated from the measured lepton momentum, $E_{\mathrm{t}}^{\mathrm{miss}}$ vector and the nominal W boson mass. We have also used a cut on $E_{\mathrm{t}}^{\mathrm{miss}}$ for high Higgs mass analysis where the $E_{\mathrm{t}}^{\mathrm{miss}}$ is significantly larger for signal than the $E_{\mathrm{t}}^{\mathrm{miss}}$ for the background. We found $E_{\mathrm{t}}^{\mathrm{miss}} > 60$ GeV is an optimum cut for 600 and 800 GeV Higgs masses to have a good background rejection.

In each case a mass window of 65 GeV $< m_W <$ 100 GeV is used to select the events. Furthermore a hard cut is introduced on the transverse momentum of the reconstructed W from the hadronic and leptonic decay products. For the $m_H = 300$ GeV signal, the reconstructed hadronic W is required to have $p_{\rm t}^{W\to jj} > 100$ GeV. For higher masses ($m_H = 600$ and 800 GeV) we have both used a cut on the transverse momentum of a reconstructed W from hadronic and leptonic decay products ($p_{\rm t}^{W\to jj} > 200$ GeV and $p_{\rm t}^{W\to l\nu} > 200$ GeV). As W is produced with a higher transverse momentum in the signal than in the background, $p_{\rm t}$ cut reduces the background even further.

The signal events, due to color coherence in the production, have a small hadronic activity in the central region. On the contrary, the background channels, especially $t\bar{t}$ events, have a significant central jet activity. We introduced the central jet veto for these events which clearly reduces the background effectively. We demand events to have no extra jets in the central region ($|\eta| \leq 2$) with $E_{\rm t}^{\rm jets} > 30$ GeV.

Table I shows the selection efficiencies for $m_H = 300$ GeV. The selection efficiency to reconstruct a Higgs mass is about 14% for the signal before jet tagging and central jet veto. At this level of analysis the background events are reduced by a factor of 15 (174) for $t\bar{t}$ (W + jets). Jet tagging brings a factor of 79 for $t\bar{t}$ and 230 for W + jets. Furthermore central jet veto reduces the $t\bar{t}$ (W+jets) background by factors of 12 (4). Similar suppression factors by the jet tagging and the central jet veto are obtained for higher Higgs masses as seen in Table II. For all the Higgs mass regions we investigated, jet tagging together with central jet veto reduces the background almost by a factor of 1000 after the reconstruction of Higgs from WW system.

For higher Higgs masses ($m_H = 600$ GeV and $m_H = 800$ GeV), due to a large boost of the W boson, the jets from W decay tend to overlap in the central region. This effect is shown in the $E_{\rm t}$ distribution in Fig. 3 where the enhancement is seen at ~ 300 GeV due to the merging of the jets from the W decay. About 40% of events contain only one single jet. To overcome this problem, the invariant mass of the di-jet system is calculated from the calorimeter cells in a larger cone and the di-jet system is required to have $E_{\rm t} > 200$ GeV. The final W mass distribution is obtained combining events with $|m_{jj} - m_W| < 2\sigma_m$ ($W \to 2$ jets), where σ_m is the resolution on the W mass, and events with the calorimeter cluster mass ($W \to 1$ jet). With the addition of events which have merged jet, the efficiency of W reconstruction is increased from 40% to about 66%.

The efficiency and resolution for reconstructing high $p_{\rm t}$ $W \to jj$ decays, the $E_{\rm t}^{\rm miss}$ resolution and the reconstruction of the longitudinal momentum of the neutrino, using the W mass constraint are the main concerns for the Higgs mass reconstruction in $H \to l\nu jj$ signal. The central jet veto cut and

TABLE I

Event selection for $H \to WW \to l\nu jj$ for $m_H = 300$ GeV.

Cuts	Signal	$t\bar{t}$	$W + \text{jets}$
$\sigma \times$ BR	0.14 pb	90.7 pb	781.4 pb
Events for 30 fb^{-1}	7815	4.89×10^6	2.11×10^7
Lepton selection	5367	2.5×10^6	9.7×10^6
Central jet selection	1260	400061	134442
Higgs reconstruction from WW system	1098	322751	121204
Tagging jet selection	180	4079	527
Central jet veto	142	342	147
m_H window $250 < m_H < 360$ GeV	121	98	42

TABLE II

Event selection for $H \to WW \to l\nu jj$ for $m_H = 600$ GeV.

Cuts	Signal	$t\bar{t}$	$W + \text{jets}$
$\sigma \times$ BR	0.03 pb	90.7 pb	108.6 pb
Events for 30 fb^{-1}	1599	4.89×10^6	2.9×10^6
Lepton selection	1308	2.5×10^6	1.7×10^6
Central jet selection	679	105973	110347
Central jet veto	443	12928	72769
Higgs reconstruction from WW system	221	2281	8497
Tagging jet selection	66	29	76
m_H window $450 < m_H < 750$ GeV	56	15	38

the forward jet tagging can be used with a high efficiency. As an important remark, in Fig. 5, Higgs mass for signal ($m_H = 600$ GeV) is superimposed on the summed signal+background is shown. In this distribution, the signal is very much suppressed against background. At the end of this study, one can compare the Higgs mass in this figure with the mass after jet tagging and then, it can be figured out how the tagging jets help to distinguish signal from background.

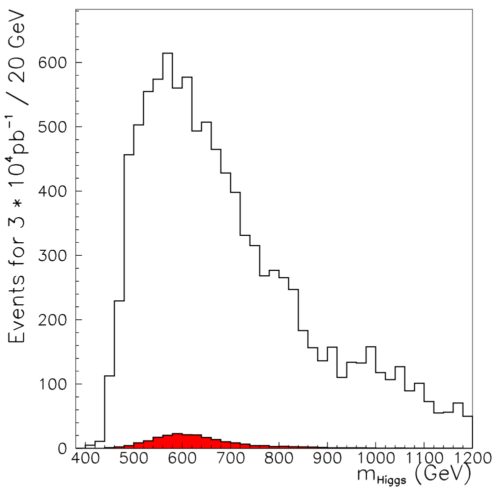

Fig. 5. Higgs mass distributions from $H \to WW \to l\nu jj$ with $m_H = 600$ GeV. The signal superimposed on the summed signal + background.

The final sample of events are selected by requiring a mass window on the Higgs masses. We require $250 < m_H < 360$ GeV and $450 < m_H < 750$ GeV for $m_H = 300$ GeV and $m_H = 600$ GeV cases, respectively.

3.2. $H \to ZZ \to lljj$, $H \to ZZ \to ll\nu\nu$

The selection of $H \to ZZ \to lljj$ events is very similar to the selection of WW events. Here we require two high p_{t} leptons with $p_{\mathrm{t}}^l > 30$ GeV. The Z mass from these two leptons is required to be within $m_Z \pm 6$ GeV. Fig. 6 (right panel) shows a Z mass reconstruction from the two lepton final state. The central and the forward/backward jet selection is exactly the same as in the WW case. In the ZZ case we only deal with the largest background, Z+jets. The forward jet tagging and the central jet veto reduce this background with a similar factor as in the case of $W +$ jets. Table III and Table IV show the event selection for $H \to ZZ \to lljj$ channel.

The $H \to ZZ \to ll\nu\nu$ channel is characterized by the two high p_{t} leptons and a large missing energy from $Z \to \nu\nu$. For this channel, a careful inves-

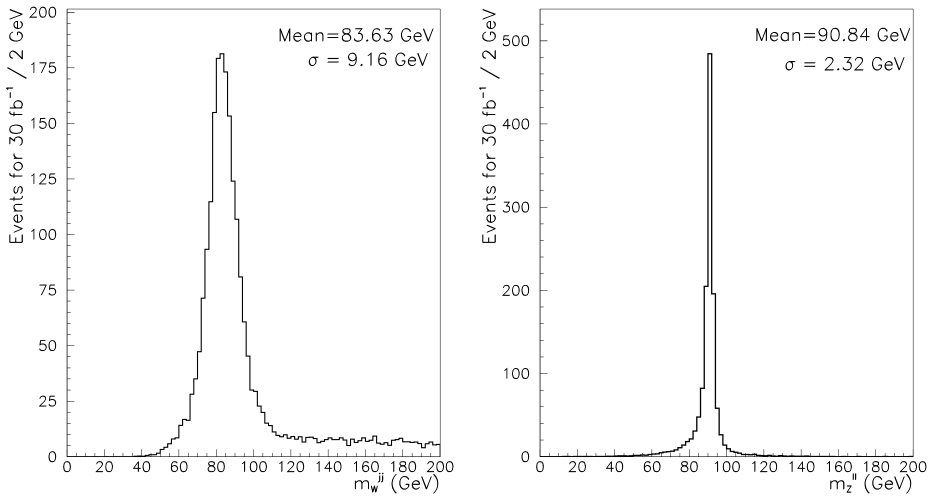

Fig. 6. Distribution of W mass reconstructed from two central jets (left figure) and distribution of Z mass reconstruction from two leptons (right figure).

TABLE III

Event selection for $H \to ZZ \to lljj$ and $H \to ZZ \to ll\nu\nu$ for $m_H = 300$ GeV. The central jet selection, the central jet veto and m_H window cut are not used in the $H \to ZZ \to ll\nu\nu$ analysis.

Cuts	$H \to ZZ \to lljj$	$Z + \text{jets}$	$H \to ZZ \to ll\nu\nu$	$Z + \text{jets}$
$\sigma \times$ BR	0.04 pb	105.6 pb	0.008 pb	105.6 pb
Events for 30 fb^{-1}	2234	2.85 $\times 10^6$	428	2.85 $\times 10^6$
Lepton selection	1321	961354	250	959434
Z mass window	1067	702172	205	700030
Central jet selection	250	26393		
$E_{\rm t}^{\rm miss} > 100$ GeV			111	2559
Higgs reconstruction from WW system	250	26393		
Tagging jet selection	41	171	19	29
Central jet veto	31	43		
m_H window $250 < m_H < 360$ GeV	29	14		

TABLE IV

Event selection for $H \to ZZ \to lljj$ and $H \to ZZ \to ll\nu\nu$ for $m_H = 600$ GeV. The central jet selection, the central jet veto and m_H window cut are not used in the $H \to ZZ \to ll\nu\nu$ analysis.

Cuts	$H \to ZZ \to lljj$	$Z + \text{jets}$	$H \to ZZ \to ll\nu\nu$	$Z + \text{jets}$
$\sigma \times \text{BR}$	0.009 pb	13.5 pb	0.002 pb	13.5 pb
Events for 30 fb^{-1}	498	413544	95	413544
Lepton selection	402	211501	76	211501
Z mass window	318	150908	61	150908
Central jet selection	156	8043		
Central jet veto	104	4677		
$E_{\rm t}^{\rm miss} > 150$ GeV			52	515
Higgs reconstruction from WW system	72	1071		
Tagging jet selection	25	12	11	4
m_H window	21	6.2		

tigation of the $Z + \text{jets}$ background is needed where the missing $E_{\rm t}$ arises from neutrinos in the jets or from mismeasured energies due to cracks or other detector effects. We expect to detect the signal in the missing energy distribution on top of the background as shown in Fig. 7. We use the same central cuts for leptons and the same mass window for the Z mass reconstruction. The only special criteria we used in this analysis is the cut on the $E_{\rm t}^{\rm miss}$. The large background suppression is shown to be achieved using the effective $E_{\rm t}^{\rm miss}$ cut. Therefore, the central jet veto is not anymore as effective as in $H \to WW \to l\nu jj$ and $H \to ZZ \to lljj$. As shown as empty entries in Table III and Table IV, we did not consider vetoing the central jets at all for $H \to ZZ \to ll\nu\nu$ analysis. Due to low statistics the m_H window cut is not applied to ZZ events in the $ll\nu\nu$ final state.

We used a cut $E_{\rm t}^{\rm miss} > 100$ GeV for events with $m_H = 300$ GeV and $E_{\rm t}^{\rm miss} > 150(200)$ GeV for higher mass $m_H = 600(800)$ GeV Higgs events. In the $H \to ZZ \to ll\nu\nu$ decay, there is more $E_{\rm t}^{\rm miss}$ expected (Fig. 7). This allows us to apply harder cuts on the missing energy. The $Z + \text{jets}$ background has a steeply falling missing $E_{\rm t}$ distribution. This feature brings a significant suppression (a factor of ~ 300) on the background. The only

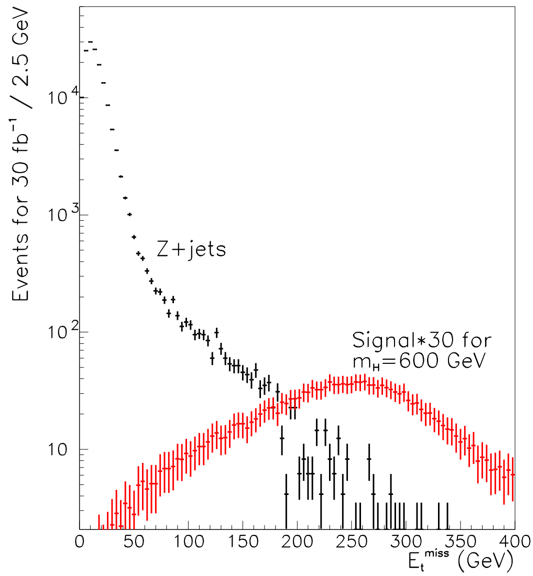

Fig. 7. Missing transverse energy, $E_{\mathrm{t}}^{\mathrm{miss}}$ distribution for the $H \to ZZ \to ll\nu\nu$ signal and the $Z+$jets background.

other main suppression factor for these events comes from the jet tagging. Jet tagging brings an additional suppression factor of about 100 for the background. The event selection for $ZZ \to ll\nu\nu$ channel are given in Table III and Table IV.

In the ZZ case, the main contributions to the experimental resolutions on the Higgs mass come from the $Z \to jj$ and the $E_{\mathrm{t}}^{\mathrm{miss}}$ reconstruction. The central jet veto cut and the forward jet tagging can still be used with a high performance in rejecting the background against the signal.

We have also calculated the signal and background events for the high Higgs mass ($m_H = 800$ GeV) case. The event selection algorithm is the same as in the case of $m_H = 600$ GeV. The result of this analysis is given in Table V for the three channels which we have investigated.

The significances and expected discovery luminosities have been evaluated using the Gaussian $S/\sqrt{B}$ approximation in Table VI and Table VII. The statistical significances are also calculated using Poisson statistics and expressed in Gaussian σ units in the numbers in parenthesis in Table VI for small event rates where signal and background events are less than 25. Poisson calculations show that for small number of events (< 25) in the ZZ analysis, the sensitivity is overestimated as much as 30%.

TABLE V

Signal and background for $H \to WW/ZZ$ with $m_H = 800$ GeV.

Channel	Signal	$t\bar{t}$	W or $Z+$jets
$H \to WW \to l\nu jj$ $\sigma \times \mathrm{BR} = 0.015$ pb	53	20	53
$H \to ZZ \to lljj$ $\sigma \times \mathrm{BR} = 0.005$ pb	16		6.2
$H \to ZZ \to ll\nu\nu$ $\sigma \times \mathrm{BR} = 0.0009$ pb	6.4		4.1

TABLE VI

$S/\sqrt{B}$ for an integrated luminosity of 30 fb^{-1}. The numbers in parenthesis show the significances calculated using Poisson statistics.

Channel	$m_H = 300$ GeV	$m_H = 600$ GeV	$m_H = 800$ GeV
$H \to WW \to l\nu jj$	10.3	7.8	6.2
$H \to ZZ \to lljj$	7.8 (6.2)	8.5 (6.1)	6.3 (4.8)
$H \to ZZ \to ll\nu\nu$	3.6 (3.2)	5.5 (4.1)	3.2 (2.3)

4. Results

We have investigated three channels for the Standard Model Higgs observation with masses between 200–800 GeV in weak boson fusion. We have shown that the forward jet tagging together with central jet veto is very efficient way to suppress the main backgrounds ($t\bar{t}$ and $W/Z+$jets). The most significant channel is the $H \to WW \to l\nu jj$ where the 5σ observation is possible with 7 to 20 fb^{-1} luminosity for Higgs masses between 300 to 800 GeV. $H \to ZZ \to lljj$ signal is also a promising clear channel where the

TABLE VII

Expected luminosities in fb^{-1} for 5σ discovery.

Channel	$m_H = 300$ GeV	$m_H = 600$ GeV	$m_H = 800$ GeV
$H \to WW \to l\nu jj$	7.1	12.3	19.5
$H \to ZZ \to lljj$	12.3	10.4	18.9
$H \to ZZ \to ll\nu\nu$	57.8	24.8	73.2

5σ observation is possible between 12 to 19 fb^{-1} luminosity for Higgs masses between 300 to 800 GeV. For $H \to ZZ \to ll\nu\nu$ signal we have obtained the best result for the Higgs mass of 600 GeV where the 5σ observation is only possible with about 25 fb^{-1} luminosity.

In this analysis the most significant signal is the $H \to WW \to l\nu jj$ with Higgs mass of 300 GeV. The $H \to ZZ$ channel gives the best results for Higgs mass of 600 GeV in either $lljj$ or $ll\nu\nu$ final states.

We are able to reconstruct the Higgs mass from both $H \to WW \to l\nu jj$ and $H \to ZZ \to lljj$ channels. The Higgs mass peak is clearly visible over the background in 300–600 GeV signals. Fig. 8 and Fig. 9. show the final Higgs mass reconstruction (for $m_H = 300$ GeV and $m_H = 600$ GeV) for the $l\nu jj$ and $lljj$ final states from W and Z decays. As the shape of the background for WW and ZZ mass reconstruction is similar to the signal shape, a good knowledge of the background remains to be essential for a direct observation of the Higgs signal through a mass peak.

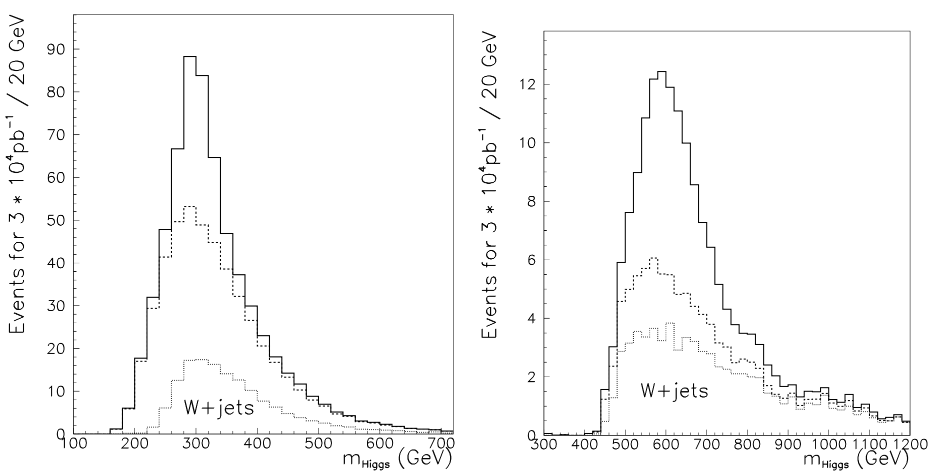

Fig. 8. Higgs mass distributions from $H \to WW \to l\nu jj$ with $m_H = 300$ GeV (left figure) and $m_H = 600$ GeV (right figure). The summed signal + background (solid histogram) is superimposed on the total background, $t\bar{t}$ and $W+$jets (dashed histogram). $W+$jets background is shown separately in the figure.

The mass resolutions from $m_H = 300$ GeV to $m_H = 600$ GeV increases as seen in Fig. 8 and Fig. 9. This is due to the large natural Higgs width for these Higgs boson masses. The width for higher masses, $m_H \sim 800$ GeV is broader.

The critical concerns in this analysis are the detector performances for reconstructing W from jj decay, the efficiency of $E_{\rm t}^{\rm miss}$ measurements and the central jet veto. The good energy measurement of tagging jets is also

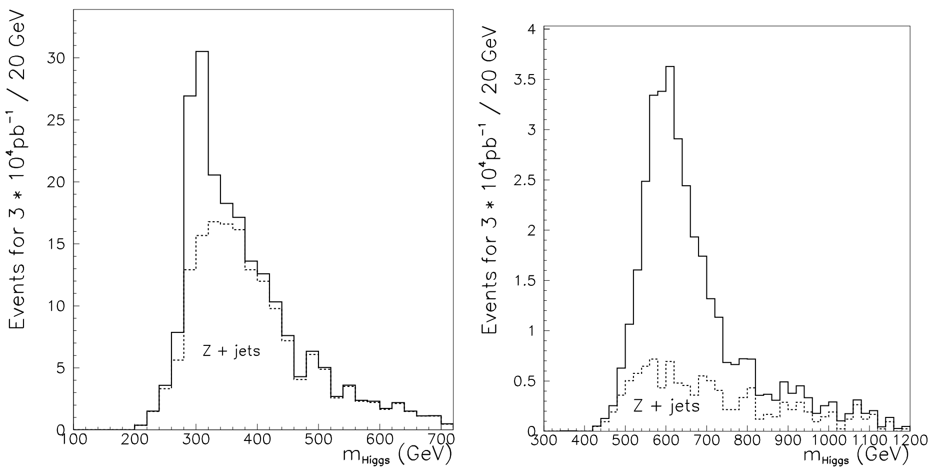

Fig. 9. Higgs mass distributions from $H \to ZZ \to lljj$ with $m_H = 300$ GeV (left figure) and $m_H = 600$ GeV (right figure). The summed signal+background (solid histogram) is superimposed on the background, $Z +$ jets (dashed histogram).

essential to suppress the backgrounds effectively. The design and the performance tests prove that [3, 14] the calorimeter quality of the CMS detector would be sufficient to meet the requirements of the analysis described in this study.

The expected statistical significance, $S/\sqrt{B}$, for 30 fb^{-1} *versus* Higgs mass for the three channels considered in this analysis are shown in Fig. 10.

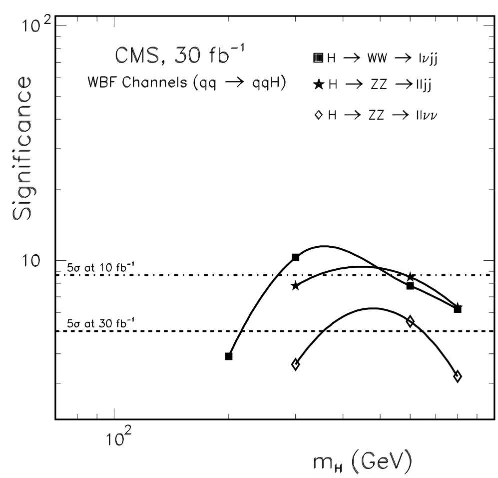

Fig. 10. The expected statistical significance for 30 fb^{-1} *versus* Higgs mass.

In our study we have also considered the WW channel for lower Higgs masses. Our simulation shows that it is still possible to obtain a good signal to background ratio ($S/\sqrt{B} = 3.9$) for $m_H = 200$ GeV in the $H \to WW \to l\nu jj$ channel. But, the significance of the signal is steeply decreasing below $m_H = 200$ GeV. The analysis cuts for $m_H = 200$ GeV case are the same as $m_H = 300$ GeV except for the required Higgs mass window. The Higgs mass window cut is $140 < m_H < 250$ GeV for $m_H = 200$ GeV analysis.

Furthermore, we have also shown in our previous study [13] the observability of Higgs signal ($m_H = 120$ GeV) at CMS in the weak boson process through the decay $H \to WW^* \to l\nu l\nu$. Although the rates are low at $m_H = 120$ GeV, it is still possible to observe the signal in a clear topology with forward tagged jets. As shown in [13], for $m_H = 120$ GeV Higgs a 5σ discovery can be possible in the low luminosity runs in the beginning of the LHC operations.

5. Conclusions

In this analysis, we have demonstrated that it is possible to observe high mass Higgs bosons in the weak boson fusion channels with its distinct characteristics under low luminosity running conditions at the CMS experiment at LHC. Observations of the isolated high p_{t} leptons between the forward jets enhances the experimental signatures for $H \to WW/ZZ$ decays. The presence of the forward jets strongly rejects the backgrounds from $t\bar{t}$ and $W/Z+$jets. The Higgs boson would be observable in the $H \to WW \to l\nu jj$, $H \to ZZ \to lljj$ and $H \to ZZ \to ll\nu\nu$ in the mass range from 300 to 800 GeV. This observation would require between 10 to 20 fb^{-1} for the CMS detector.

For the Standard Model, $gg \to H \to ZZ/ZZ^* \to 4l^{\pm}$ remains to be the cleanest signature where the Higgs mass measurement can be done with a very good precision by the excellent four-lepton mass resolution. On the other hand, if the $H \to WW^* \to l\nu l\nu$ channel is considered as a potential channel for the mass range below 200 GeV down to the LEP II limit, together with the result of this study for higher Higgs boson masses, $m_H > 200$ GeV, the weak boson fusion channels can also be the most promising channels for detecting the Standard Model Higgs Boson over a large range of masses with a good accuracy.

We would like to thank D. Denegri and R. Kinnunen for their continuous support and valuable comments during this study.

REFERENCES

[1] The ALEPH, DELPHI, L3 and OPAL Collaborations, and the LEP Higgs Working Group, CERN-EP/2001-055; `hep-ex/0107030`.

[2] The LEP Electroweak Working Group, A Combination of Preliminary Electroweak Measurements and Constraints in the Standard Model, D. Charlton, EPS HEP 2001, Budapest, Hungary, July 12–18, 2001. See http://www.hep2001.elte.hu

[3] CMS Collaboration, The Hadron Calorimeter Project, Technical Design Report, CERN/LHCC 97-31, CMS TDR 2, 20 June 1997.

[4] S. Abdullin, N. Stepanov, CMS TN/94-178.

[5] ATLAS Collaboration, ATLAS Detector and Physics Performance Technical Design Report, CERN/LHCC/99-19.

[6] W.J. Stirling *et al.*, *Phys. Lett.* **B163**, 261 (1985); D. Dicus *et al.*, *Phys. Rev.* **D37**, 2474 (1988).

[7] V. Cavasinni *et al.*, ATL-PHYS-98-127.

[8] D. Rainwater, D. Zeppenfeld, *Phys. Rev.* **D60**, 113004 (1999); N. Kauer *et al.*, *Phys. Lett.* **B503**, 113 (2001).

[9] K. Iordanidis, D. Zeppenfeld, *Phys. Rev.* **D57**, 3072 (1998).

[10] T. Sjostrand, *Comp. Phys. Commun.* **82**, 74 (1994); CERN-TH.6488/92; CERN-TH.7112/93.

[11] S. Abdullin *et al.*, CMSJET, CMS TN/94-180.

[12] H.D. Yıldız *et al.*, CMS-NOTE/2001-050.

[13] N. Akchurin *et al.*, FERMILAB-FN-714, February 2002, CMS-NOTE/2002-016; CMS Internal NOTE/2002-066.

[14] N. Akchurin *et al.*, *Nucl. Instrum. Methods Phys. Res.* **A399**, 202 (1997).